GeoConvention
Calgary • Canada • March 7-11 2016
OPTIMIZING RESOURCES

Constraining low-frequency acoustic impedance inversion by using reflection stacking velocities

Yichuan Wang and Igor B. Morozov
University of Saskatchewan

Summary

Reflection seismic data are often transformed into acoustic-impedance (AI) pseudo-logs for quantitative reservoir prediction. As AI equals the product of density and P-wave velocity, it has the benefit of representing a rock property instead of interface property such as reflection amplitude. By combining seismic AI inversions with spectral information from well logs, high-quality AI pseudo-logs volumes can be produced by the Seismic by Interpolated-Log Calibration (SILC) method (Morozov and Ma, 2009). However, a well-known difficulty of all AI inversion methods consists in the lack of low-frequency information in seismic records. Here, we investigate ways for deriving this information from the results of seismic processing, such as the interval, stacking, or migration velocities. Low-frequency impedance calculated from these velocities are calibrated by the available impedance calculated from acoustic-log velocities in order to provide empirical dependences. These dependences can be further extrapolated to 3-D data volumes in SILC or any other types of AI inversion. The approach is illustrated on a 3-D 3-C dataset from Weyburn CO_2 sequestration project in southern Saskatchewan.

Introduction

The SILC method is a simple and effective way to produce AI pseudo-log volumes. This method combines the AI inverted from seismic data, spectral information from well logs and low-frequency AI also inferred from well logs. However, well logs are sparse and may inaccurately represent the spatially-variable low-frequency AI. In such cases, it could be useful to complement the low-frequency AI with velocity information derived during 3-D reflection data processing.

Here, we utilize the interval-velocity volume derived from reflection processing to calculate the low-frequency AI. The two principal difficulties of this derivation are that: 1) the low-frequency AI_{lf} is not automatically equal the AI_{int} inferred from interval velocities, and 2) the interval velocities have to be inferred from stacking velocities. Answers to these questions yield an empirical dependence of the form $AI_{lf}(AI_{int})$ derived below, which can be further used in any type of AI inversion. Similarly to the SILC method, the dependence $AI_{lf}(AI_{int})$ is derived by calibration using the available well logs.

Method

To derive the $AI_{lf}(AI_{int})$ dependence, a common mid-point (CMP) nearest to the well location is considered. For a horizontally-layered velocity structure, the stacking velocity used for NMO correction equals the root-mean-square (RMS) velocity V_{rms}, which is related to the interval velocities V_{int}:

$$V_{rms}^2(t) = \frac{1}{t}\int_0^t V_{int}^2(\tau)d\tau. \quad (1)$$

To estimate the low-frequency AI, the $V_{int}(t)$ must be a continuous function. Such a continuous, piecewise-linear function can be parameterized as a linear combination of basis functions $\varphi_i(t)$ shown in red in Figure 1 (the Rayleigh-Ritz method; Aki and Richards, 2002):

$$V_{int}^2(t) = \sum_{i=1}^{N_m} \varphi_i(t)\, m_i, \tag{2}$$

where m_i are unknown parameters, with i = 1…N_m.

From equations (1) and (2), the squared RMS velocity is also a linear combination of parameters m_i:

$$V_{rms}^2(t) = \sum_{i=1}^{N_m} \psi_i(t)\, m_i, \tag{3}$$

where $\psi_i(t) = \frac{1}{t}\int_0^t \varphi_i(\tau)d\tau$ is another set of basis functions (blue in Figure 1).

Let us denote t_j the times at which the stacking velocities $V_{stack}(t_j)$ are picked from reflection CMP gathers. At these times eq. (3) must satisfy $V_{stack}(t_j) = V_{rms}(t_j)$, which can be written in matrix form as:

$$\mathbf{d} = \mathbf{Lm}, \tag{4}$$

where vector $\mathbf{d}$ consists of the squared stacking velocities: $d_j = V_{stack}^2(t_j)$ and the elements of matrix $\mathbf{L}$ equal $L_{ij} = \psi_i(t_j)$. The least-squares solution for $\mathbf{m}$ is:

$$\mathbf{m} = (\mathbf{L}^\mathbf{T}\mathbf{L})^{-1}\mathbf{L}^\mathbf{T}\mathbf{d}. \tag{5}$$

With this estimated model vector $\mathbf{m}$, the squared interval and RMS velocities at any time t are predicted by equations (2) and (3), respectively.

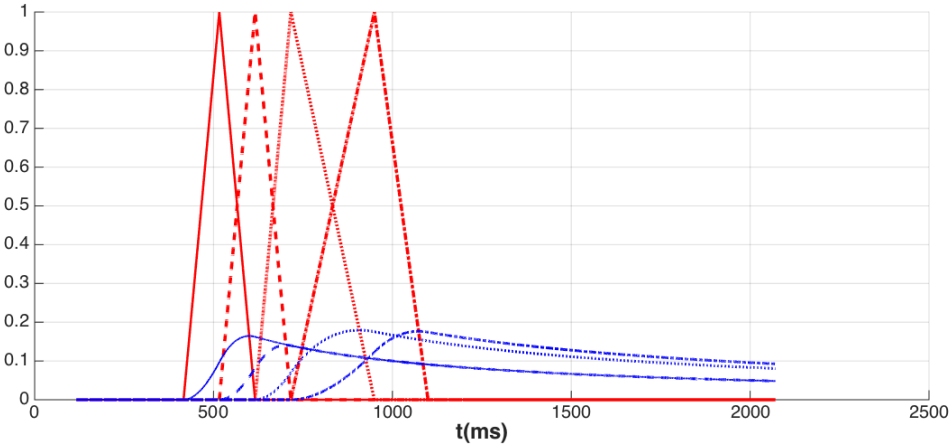

Figure 1: Basis functions $\varphi_i(t)$ (red) and $\psi_i(t)$ (blue) in equations (2) and (3) for four consecutive values of i.

Using the obtained interval velocity in eq. (2), the density is approximated by the Gardner equation (Gardner et al, 1974):

$$\rho = \alpha V^\beta, \tag{6}$$

where V is measured in m/s and ρ is the density given in g/cm^3. For the area of this study, we estimate $\alpha \approx 0.25$ and $\beta \approx 0.28$. Then the AI is calculated as:

$$AI = \alpha V^{(1+\beta)}. \tag{7}$$

Generally, the AI calculated by eq. (7) using V_{int} may differ from the low-frequency AI_{lf}. To infer an empirical relation between AI_{lf} and AI_{int}, we consider a cross-plot of the low-frequency AI calculated from V_{int} and the AI calculated by using the same eq. (7) from a P-wave velocity log. By interpreting this cross-plot, we infer an empirical dependence $AI_{lf}(AI_{int})$, which can be further utilized as a low-frequency constraint on AI calculations.

Application

The approach is applied to 3-D 3-C prestack seismic data from Weyburn CO_2 sequestration project in southern Saskatchewan (White, 2009). Stacking velocities obtained during seismic data processing (Gao, 2011) in an area adjacent to the well were transformed into interval velocities by using the method in eqs. (2)-(5) (Figure 2). This procedure is sensitive to the selection of the control points determining the sets of basis functions $\varphi_i(t)$ and $\psi_i(t)$. This sensitivity was examined by performing 100 random perturbations (range from -50 to 50ms) of the positions of control points and the initial positions of control points were set at 120, 250, 450, 550, 650, 750, 1000, 1150, 1300, 1450, 1650, 1750 and 2150ms determined from the number and positions of stacking velocities picked from reflection data. Each of these perturbations produces an interval-velocity curve (black) and RMS-velocity curve (red) in Figure 2. Finally, median values were calculated from all 100 interval-velocity curves, resulting in an estimated $V_{int}(t)$ (yellow curve in Figure 2).

To obtain an empirical relation for the low-frequency AI_{lf}, we try deriving it as a function of AI_{int} irrespective of the observation time. In Figure 3, the low-frequency AI calculated from $V_{int}(t)$ is cross-plotted against the AI calculated from P-wave velocity from well log by using eq. (7). For the shallow part, AI_{int} is almost equal the average AI in the log. Between AI levels of about 5000 to 9000 m/s*g/cm^3, the average log AI appears to be slightly below AI_{int}, and above about 9000 m/s*g/cm^3, the log AI appears systematically larger than AI_{int}. Potentially, this underestimation of the AI_{int} at larger depths is related to the poor resolution of stacking velocities and tendency for the processor to pick at the lower end of the velocity uncertainty range.

The interpreted empirical dependence $AI_{lf}(AI_{int})$ is shown by the red line in Figure 3. This dependence should be useful for enhancing the accuracy of several types of impedance inversions. Although calibrated at a single available well (Figure 3), this dependence can be applied to variable stacking- and interval-velocity profiles within the 3-D study area.

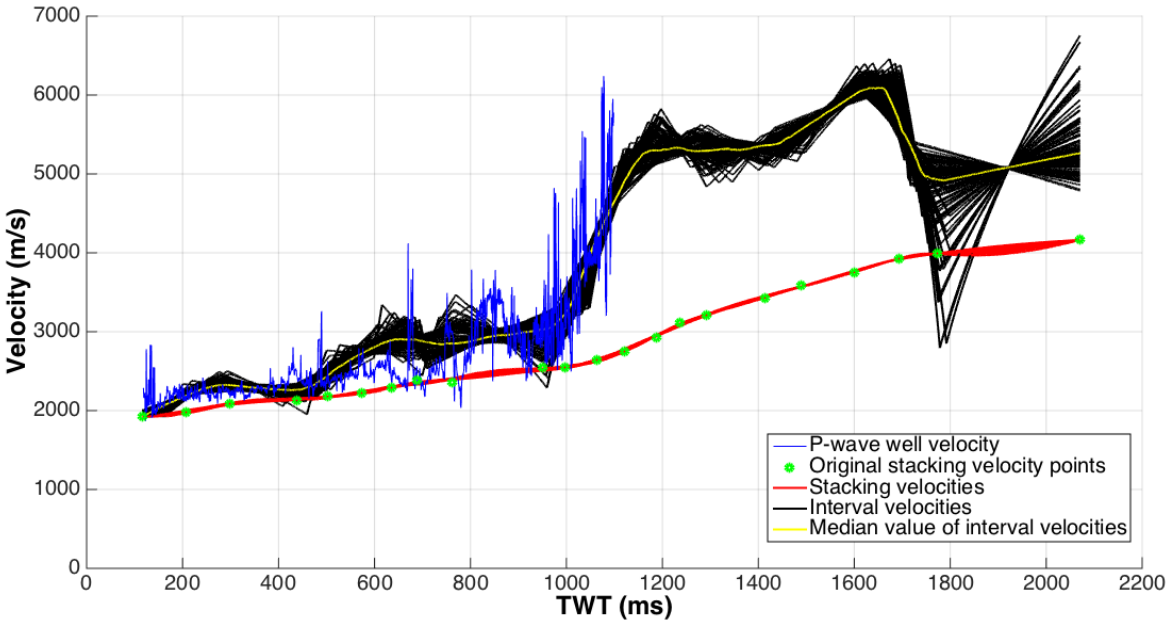

Figure 2: Seismic velocities for a location adjacent to well 102042300614 and well-log velocity of this well. Green dots are the stacking velocities picked from reflection data, and blue curve is the P-wave velocity from the well log. Black lines are the interval velocities, which are predicted by eq. (2) with different randomizations of control points, and yellow curve is their median value at each time. Red curves are the RMS velocities predicted by eq. (3).

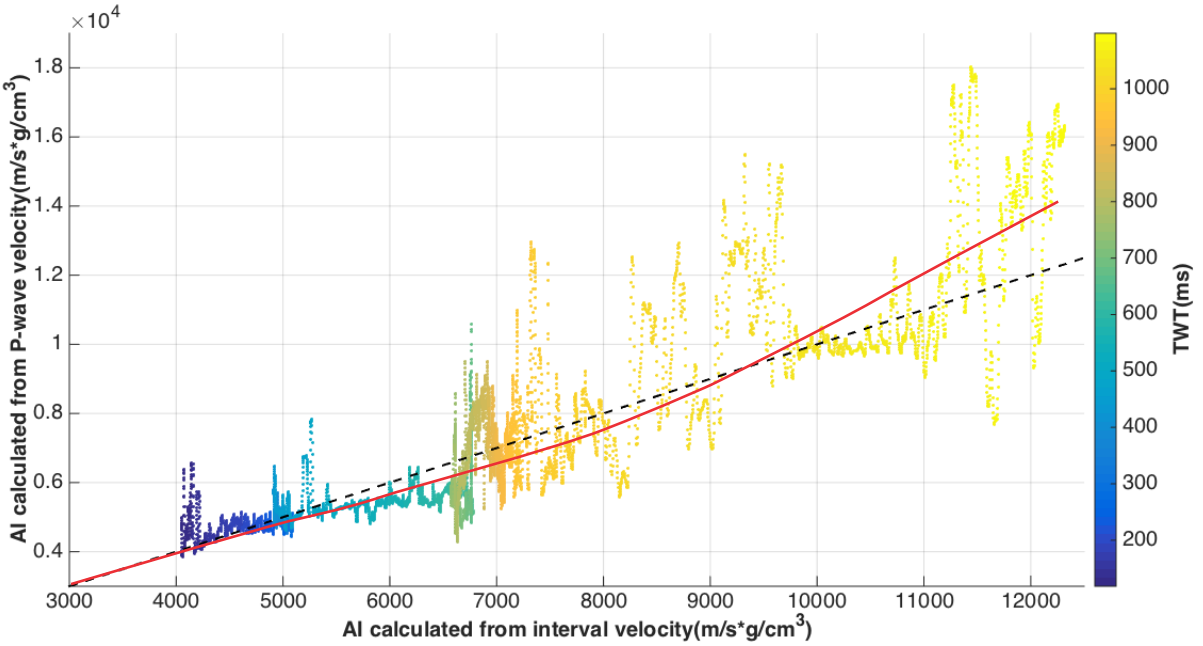

Figure 3: Correlation of the AI inferred from seismic data analysis (horizontal axis; AI_{int}) with AI inferred from velocities in situ (vertical axis; AI). Color bar on the right shows the two-way travel time. Black dashed line is a reference line corresponding to $AI = AI_{int}$. Red line is the empirical dependence $AI_{lf}(AI_{int})$ interpreted from this cross-plot.

Conclusions

Velocities inferred from seismic processing can be used to enhance the accuracy of low-frequency acoustic impedance (AI) inversion. By inverting continuous distributions of interval velocities with depth and calibrating them by using well-log data, empirical estimates for the spatially-variable, low-frequency AI can be made and utilized in many AI inversion schemes.

References

Aki, K. and P. G. Richards, 2002. Quantitative Seismology, 2th ed., University Science Books.

Gardner, G. H. F., Gardner, L. W. and A. R. Gregory, 1974. Formation velocity and density—the diagnostic basics for stratigraphic traps, Geophysics, **39**(6), p. 770-780.

Gao L. and I. B. Morozov, 2011. AVO Analysis of 3-D/3-C Datasets from Weyburn CO_2 Storage and Monitoring Project, 2011 CSPG/CSEG/CWLS Convention.

Morozov, I. B. and J. Ma, 2009. Accurate poststack acoustic-impedance inversion by well-log calibration, Geophysics, **74**(5), R59-R67.

White, D., 2009. Monitoring CO_2 storage during EOR at the Weyburn-Midale Field, The Leading Edge, **28**(7), p. 838-842.